JOURNAL OF PROPULSION AND POWER
Vol. 23, No. 4, July–August 2007

Vitiation Effects on Scramjet Engine Performance in Mach 6 Flight Conditions

Sadatake Tomioka,* Tetsuo Hiraiwa,† Kan Kobayashi,‡ and Muneo Izumikawa§
Japan Aerospace Exploration Agency,
Kimigaya, Kakuda, Miyagi 981-1525, Japan
and
Tomoyuki Kishida¶ and Hiroyuki Yamasaki**
Tokyo Institute of Technology, Nagatsuta, Midori-ku, Yokohama, Kanagawa 226-8502, Japan

DOI: 10.2514/1.28149

Quasi-one-dimensional analyses with either chemical equilibrium or finite-rate reaction were conducted to evaluate the effects of contamination due to flow vitiation on engine performances, namely, thrust production. The incoming flow state was calculated based on measurements, and a higher total enthalpy for the freestream through a vitiation heater compared to that through a storage heater was found, the difference in the flow condition being responsible for two-thirds of the reduction in the thrust production with vitiation observed in the engine tests. With the finite-rate reaction calculation, the possibility of a further reduction due to the contamination effect on the combustion mechanism was found, which was responsible for one-third of the measured reduction. The one-dimensional analyses were further pursued to find matched test conditions with the storage heater to that with the vitiation heater in view of the thrust production and pressure distribution within the engine, and both freestream enthalpy and fuel equivalence ratio should be adjusted to attain the matched conditions.

Nomenclature

A	=	cross-sectional area
E	=	total enthalpy
F, ΔF	=	thrust, thrust increment
G_f	=	fuel mass flow rate
p, q	=	static pressure, dynamic pressure
t, Tt	=	static temperature, and total temperature
X, Y	=	streamwise location from imaginative leading edge of side-wall, spanwise location from duct center
X'	=	streamwise distance from injector location
X'_ϕ	=	streamwise distance required to attain complete mixing for an equivalence ratio of ϕ
η_c, η_m	=	combustion efficiency, mixing efficiency
ϕ	=	equivalence ratio

Subscripts

a	=	freestream
i	=	initial
ref	=	reference state
S, V	=	storage heater mode, vitiation heater mode
w	=	wall
0, 1	=	in facility plenum chamber, at entrance of engine

Presented as Paper 5038 at the 42nd AIAA/ASME/SAE/ASEE Joint Propulsion Conference and Exhibit, Sacramento, CA, 9–12 July 2006; received 3 October 2006; revision received 26 March 2007; accepted for publication 29 March 2007.

*Section Leader, Combustion and Control Section, Combined Propulsion Research Group, Institute of Aerospace Technology, Kakuda Space Center. Senior Member AIAA.

†Associate Senior Researcher, Combined Propulsion Research Group, Kakuda Space Center. Member AIAA.

‡Researcher, Combined Propulsion Research Group, Kakuda Space Center. Member AIAA.

§Associate Senior Researcher, Combined Propulsion Research Group, Kakuda Space Center.

¶Graduate School Student, Interdisciplinary Graduate School of Science and Engineering, Department of Energy Science.

**Professor, Interdisciplinary Graduate School of Science and Engineering, Department of Energy Science. Member AIAA.

I. Introduction

THE combined-cycle engines are expected to be the most efficient propulsion system for launch vehicles and hypersonic cruise vehicles, which the Japan Aerospace Exploration Agency (JAXA) is now pursuing as long-term efforts. A candidate of the engine combination is to embed rocket engines in a supersonic combustion ramjet (scramjet) flow pass [1]. As part of the research efforts on the rocket–ramjet combined-cycle engine, a complete subscaled model of the scramjet engine has been tested at JAXA—Kakuda Space Center [2,3], using a blowdown type, semifreejet engine test facility (RamJet Engine Test Facility, RJTF). This model engine has a side-compression-type inlet, a constant cross-sectional area isolator with steps for flame holding at its exit, a constant cross-sectional area combustor with fuel injectors, a diverging area combustor, and a nozzle with rather rapid expansion. Various struts were installed for additional compression when required.

In the engine tests under M6 flight conditions [3], two different modes of combustion were observed, one designated as the "weak combustion mode" with some combustion within the boundary layer without a major rise in pressure, and the other designated as the "intensive combustion mode" with combustion within the core flow with a major rise in pressure. The gas sampling at the exit cross section of the engine revealed that combustion was rate controlled by reactions in the weak combustion mode. In the intensive combustion mode, it was rate controlled mainly by mixing, while the reaction-rate-controlling state was still observed within a minor portion of the cross section.

The M6 flight conditions can be simulated with either a storage air heater (termed as the "M6S" case) or a vitiation air (H_2 combustion) heater (termed as the "M6V" case) to investigate the effects of vitiation on engine performance. As a mixing process was found to be the governing rate-controlling factor in the Mach 6 flight condition [4], it was expected that the test media had a minor effect on the combustion process and engine performance. However, the engine showed a sizable difference in its performance with different test media, that is, a clean air in the M6S case and a vitiated air in the M6V case, even when the engine was in the intensive combustion

mode [3]. The engine showed a lower thrust in the vitiated airflow. Thus, the reaction rate and consequent time required for completion of the reaction (termed as reaction time, [3]) might have an impact on the engine performance through the combustion process.

Vitiation effects on the combustion process within hypersonic engines have been investigated since the 1960s. Recently, a thorough review of these studies was carried out by Pellet et al. [5] and a scaling method based on the Damkoeler number was proposed. One major concern was the ignition process. Among these reviewed studies, Edelmann et al. [6] made a one-dimensional assessment of the performance of a simple model scramjet engine in different test media with identical freestream Mach number, static pressure, and static temperature, to investigate the vitiation effects on the performance. Srinivasan and Erickson [7] made three-dimensional calculations on the flowfield within a supersonic combustor with different test media, and reported that the major effects of the vitiation were through thermodynamic effects. Although many analytical and numerical studies have been carried out on vitiation effects, real engine data to validate these analyses are quite scarce, the above-mentioned engine tests at the JAXA—KSPC (Kakuda Space Center) being the only one known to the authors. Upon these engine test results at the M6 flight conditions, Mitani et al. [3] conducted a zero-dimensional kinetic calculation on the above-mentioned vitiation effects, showing that the high concentration of water vapor within the M6V flow could retard the exothermic reactions. However, no quantitative evaluation of vitiation effects on engine performance was conducted.

In our previous study [8], we conducted quasi-one-dimensional analyses to evaluate the effects of chemical reaction on engine performance. By chemical equilibrium calculations, we identified the effects of the difference in the airflow condition, namely, the flow enthalpy, on the engine performance to be responsible for the $2/3$ of the difference in thrust productions. By finite-rate reaction (kinetic) calculation, we identified the effects of flow contamination through the reaction time on the engine performance to be responsible for the remaining $1/3$ of the difference. In these calculations, whole fuel was accounted for reaction, while a certain portion of the fuel was found to be unmixed even at the exit of the engine in the experiments [9], so that this portion should be accounted to be inert in the calculation. Some radicals, HO_2 and H_2O_2, were not taken into account in the previous calculation while they were reported [10] to be important species on the reaction time.

The objectives of the present study are 1) to refine the analyses for better quantification, and 2) to find matched tests conditions of the M6S and M6V cases for identical thrust production. At first, the analyses methods were modified to reflect the engine test results, namely, the measured mixing efficiency at the engine exit, and the above-mentioned results were reproduced and herein described. Then the test conditions of the M6S case, namely, the airflow enthalpy and fuel equivalence ratio, were changed to attain matched engine performance to that of the M6V case.

II. Description on the Scramjet Engine Tests

Engine tests were carried out at both M6S and M6V conditions. Airflow conditions were not agreed with each other because the same facility nozzle was used for two conditions with different thermal properties. Table 1 summarizes the flow states at the M6S and M6V conditions. Note that total temperature measurement was difficult in the M6V case, so that the tabulated value was obtained from a one-dimensional equilibrium calculation. A restriction on the storage heater operation resulted in a lower total temperature than the design

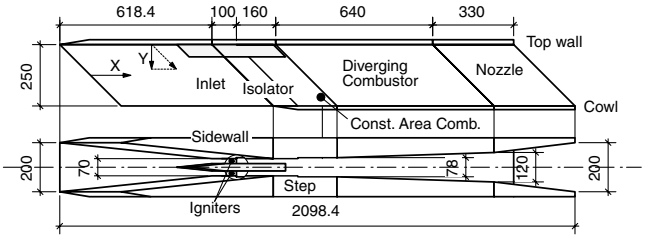

Fig. 1 Schematic of scramjet engine model.

point for the M6S case. In the present study, the freestream conditions were calculated based on the measured flow rates, the enthalpy, the static pressure, and the boundary layer momentum thickness [11]. The resulting dynamic pressures were almost identical between these two cases.

The scramjet engine was a rectangular one with a length of 2.1 m, as shown in Fig. 1. Details are found in [9]. It consisted of a cowl, a top wall, and two sidewalls. The entrance and the exit of the engine were 200 mm in width and 250 mm in height.

The inlet was a side-wall compression type with a 6-deg half-angle. The leading edge was swept back by 45 deg to deflect the freestream for spillage required in the starting sequence. The geometrical contraction ratio was 3.13 with a strut (30 mm in width and 50 mm in height) being installed on the top wall of the isolator between the inlet and the combustor for ignition and flame holding.

To reduce the inlet/combustor interaction, a constant area isolator was placed between them. The isolator was 100 mm in length. The engine had a pair of plasma torch igniters on the top wall. Backward-facing steps between the isolator and the combustor were adopted for flame holding. They were 4 mm in height on the sidewalls and 2 mm in height on the top wall. Room temperature gaseous hydrogen was injected vertically from the sidewalls through equally spaced 24 holes (1.5 mm in diameter) 30 mm downstream of the step location. A 160 mm long constant-cross-sectional-area combustor section was followed by a 640 mm long diverging combustor section, and a 330 mm long nozzle section.

Thrust, lift, and pitching moment generated by the engine were measured by using a floating-frame force measuring system (FMS). The engine thrust was evaluated with "thrust increment" ΔF, that is, the increase in the measured thrust due to injection and combustion from the airflow state. The thrust and thrust increment were normalized with dynamic pressure of the incoming freestream q_{a1} and the engine projected area A_1 to attain a thrust coefficient. The engine wall pressure was measured at 150 stations to evaluate thrust increment obtained by pressure integration. Mitani et al. [2] reported that thrust increment obtained by pressure integration agreed with that by FMS, showing that the engine internal friction was not affected by the occurrence of combustion. In the present study, pressure was normalized with q_{a1}.

The thrust increments, from both the M6S and M6V cases, are compared in Fig. 2 as functions of the fuel equivalence ratio ϕ. As will be shown later, the oxygen flow rates were almost identical in both cases, so that identical fuel flow rate means identical equivalence ratio. The equivalence ratio of unity corresponded to $G_f \sim 154$ g/s in both cases. The solid symbols show the thrust increment measured in the M6S case. The open symbols show the thrust increment measured in the M6V case. A slightly lower thrust increment was observed in the M6V case than that in the M6S case at the $\phi = 0.3$–0.4 regime. The difference due to the test medium is more apparent when we compare the limit fuel flow rates at the

Table 1 M6S and M6V flow conditions

	Supply flow rate, kg/s			Measured temp., K	Measured pres., kPa		Measured Mach no.	Calculated at nozzle exit	
	Air	H_2	O_2	Plenum	Plenum	Nozzle exit	Nozzle exit	Mach no.	Static temp., K
M6S	29.2	0	0	1480	4780	5.3	5.30 ± 0.15	5.43	232
M6V	22.7	0.35	4.33	1530[a]	4520	5.8	5.15 ± 0.15	5.21	271

[a]Estimated value with one-dimensional equilibrium calculation.

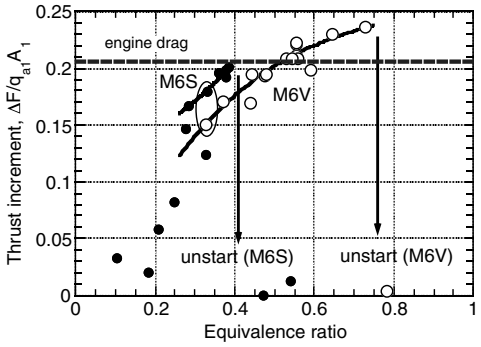

Fig. 2 Engine performances in the M6S and M6V cases.

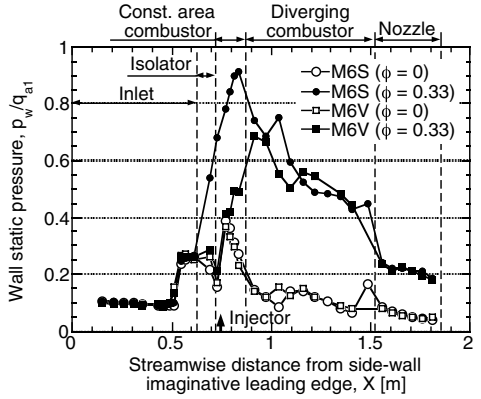

Fig. 3 Measured wall pressure distributions in the M6S and M6V cases.

engine unstart transition. The engine fell to unstart at a lower equivalence ratio in the M6S case in comparison with the M6V case, that is, the maximum ϕ for engine start in the M6S case was about 0.4, while that in the M6V case was about 0.7, and the engine thrust overcame the engine drag in the latter case.

The FMS measurement error was reported to be ± 40 N. However, the standard deviation of the thrust increment in the M6S case in the ϕ range of 0.3–0.4 shown in Fig. 2, was ± 16 N. With the dynamic pressure q_{a1} and cross-sectional area A_1 being about 110 kPa and 0.05 m^2, the estimated nondimensional error of the thrust was ± 0.003.

In the present study, we selected the M6S and M6V cases with almost identical ϕ of 0.33 (circled in Fig. 2). Figure 3 shows the measured wall pressure distributions in both the M6S and M6V cases, with or without fuel injection. The distributions without fuel injection were almost identical regardless of the test medium, while that with the injection in the M6S case clearly shows a higher peak pressure further upstream than that in the M6V case. In the latter half of the diverging combustor and in the entire nozzle, the pressure levels in both cases are almost identical.

Gas sampling was conducted in the M6S case at $G_f = 71.5$ g/s ($\phi = 0.46$) [9], and a mass-averaged combustion efficiency of 78% and a mass-averaged mixing efficiency of 83% were deduced at the engine exit. One should note that this mixing efficiency was based on the state of the specimen averaged over a certain time and space. Diskin and Northam [12] suggested an experimental correlation between the combustor geometry and fuel equivalence ratio in the following manner to calculate mixing efficiency at any streamwise distance from the injector location X' as

$$\eta_m = 1.01 + 0.176 \times \ell_n(X'/X'_\phi) \tag{1}$$

and the length for complete mixing X'_ϕ can be calculated by

$$X'_\phi/X'_{\phi\text{ref}} = 0.1791 \times \exp[1.72 \times (\phi/\phi_{\text{ref}})] \tag{2}$$

where we could use the above-mentioned $\phi = 0.46$ case as the reference condition. Using the current engine geometry and the sampling results, we could estimate the mixing efficiency as a function of the equivalence ratio. For example, the mixing efficiency at the engine exit was 87% at $\phi = 0.33$.

III. One-Dimensional Analyses

An in-house quasi-one-dimensional equilibrium calculation code [8] was used to calculate the ideal engine performance with infinite reaction rates, so as to investigate the effect of the differences in the nominal flow conditions on the engine performance. The flow was assumed to be a homogeneous mixture of the entire airflow, the fuel, and the burnt gas. Thirteen species (H, HO_2, H_2, H_2O, H_2O_2, N, NO, NO_2, N_2, O, OH, O_2, and Ar) were taken into account in the chemical equilibrium calculation within the mixture stream, HO_2 and H_2O_2 being added in the present study. In the present study, both wall friction and wall heat transfer were neglected because 1) these have little effects on the measured thrust increment as shown in the previous study [2], 2) the kinetic code used in the present study had no capability for friction estimation, 3) these were shown to have little effects on the reduction in the thrust production due to vitiation with the one-dimensional analyses (see the Appendix), and 4) for shorter calculation time. Kinetic calculations were carried out using a commercially available kinetic code (LSENS [13]) to investigate the impact of the reaction time on the engine performance.

For both the equilibrium and kinetic calculations, the mixture states at the entrance of the combustor should be given. These states were calculated with the equilibrium code, as the radicals formed in the vitiation heater would not reach the engine [14]. For both the M6S and M6V cases, a capture ratio of 0.88 [15] and a kinetic energy efficiency of 0.98 were assumed. The resulting pressure level at the exit of the isolator section was found to be in good agreement with the measured value [8]. The initial state of the mixture was calculated on the assumption that airflow and fuel completely mixed in infinitesimal distance behind the steps. The unmixed portion (13% in the present cases) of the fuel mentioned above was also taken into account to obtain the mixture state, but was assumed to be kinetically inert for both the equilibrium and kinetic calculations. As Eq. (1) shows, the mixing efficiency should increase in the streamwise direction to reach the exit value. However, the scheduled mixing and the instantaneous mixing were found to lead to the same conclusion on the vitiation effects on the engine performance ([8], see also the Appendix). Thus, the instantaneous mixing was assumed in the present study.

The step base pressure as well as the strut base pressure was assumed to be equal to the airflow static pressure, with the strut base location being aligned to the side-wall step location for simplicity of the calculation. The state quantities at the combustor entrance and after complete mixing are shown in Table 2. The oxygen flow rate was nearly equal for both conditions, so that the equivalence ratio was almost identical in both cases. However, total enthalpy in the M6V case was 9% higher than that in the M6S case.

Table 2 Combustor entrance flow states obtained with equilibrium calculation

	Fuel flow rate	Flow states at combustor entrance				O_2 flow rate	State quantity after complete mixing		
	g/s	t, K	p, kPa	Mach no.	E, GW	mol/s	t, K	p, kPa	Mach no.
M6S	50.5	408	25.3	3.84	8.6	38.6	390	22.6	3.68
M6V	50.4	456	26.5	3.76	9.4	38.7	432	23.6	3.62

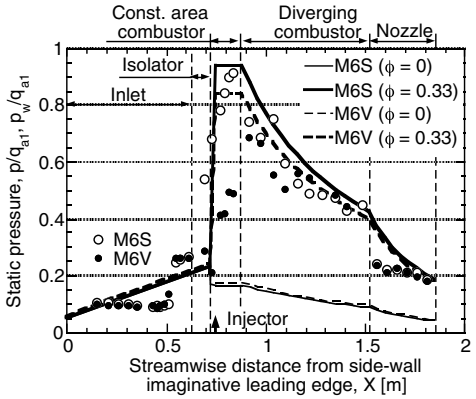

Fig. 4 Calculated static pressure distributions in the M6S and M6V cases with equilibrium code.

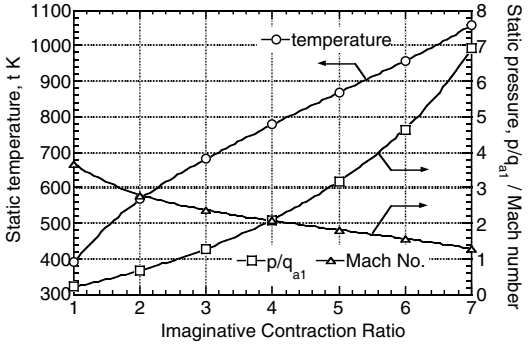

Fig. 5 Variations of static temperature, pressure, and Mach number with imaginative contraction ratio.

IV. Analysis of Engine Test Results

In this section, engine operations under the tested flight conditions were simulated with the one-dimensional analyses to investigate the cause of the obtained vitiation effects on engine performance.

A. Performance Comparison by Equilibrium Calculation

The performance prediction by the one-dimensional equilibrium calculation was carried out to evaluate the effect of the difference in the nominal flow conditions (see Table 2) on the engine performance.

Figure 4 shows one-dimensionally obtained static pressure distributions in both the M6S and M6V cases with or without fuel injection. These pressure distributions were integrated to attain thrust production in the diverging sections and are summarized in Table 3. The thrust increments were calculated by subtracting the thrust without fuel injection from that with the fuel injection, as the pressure distributions within the converging section were identical regardless of the fuel injection. As shown in Fig. 4, the peak pressure value within the constant area combustor and following pressure level in diverging sections in the M6V case with injection was about 10% lower than those in the M6S case. This difference in pressure caused the difference in the thrust increment shown in Table 3. For almost identical heat release levels, the ratio of the heat release rate against the incoming flow enthalpy was 10% lower in the M6V case than that in the M6S case, being reflected to the difference in the pressure level.

In Fig. 4, the measured values in both the M6S and M6V cases are also shown. The measured distribution in the M6S case was close to the calculated one, showing that setting the mixing efficiency to the above-mentioned value was reasonable. Discrepancies between the calculation and the measurement were at the onsets of both the diverging combustor and nozzle, where the 3-D effects were dominant. In the M6V experiments, a delay in heat release was obvious, the location of the pressure rise being shifted downstream. This delay resulted in heat release within a higher Mach number flow, and consequently, a larger total pressure loss and a higher static pressure level in the latter half of the diverging combustor and in the nozzle.

As shown in Table 3, the reduction in the thrust increment in the M6V case with respect to that in the M6S case, denoted as "thrust reduction" rate and defined as $(\Delta F_{\mathrm{M6S}} - \Delta F_{\mathrm{M6V}})/\Delta F_{\mathrm{M6S}}$, was 16% in the experiment, and 10% in the calculation. Thus, the difference in the flow condition, namely, the freestream enthalpy, was responsible for 2/3 of the thrust reduction.

B. Performance Comparison by Kinetic Calculation

Next, effects of reaction time in the M6V case were examined using the finite-rate kinetic calculation. As the initial condition for the kinetic calculation, the mixture states listed in Table 2 were used. However, no ignition occurred because static temperature and pressure, after complete mixing, was too low to initiate any reaction. Then, shock-induced combustion was explored, that is, the mixture was aerodynamically compressed through a so-called precombustion shock system [16] before the reaction zone. To simulate this situation, the same calculation method was used as for the inlet compression process, the mixture after complete mixing being compressed with an assumed kinetic efficiency of 0.98 and a full capture. The contraction ratio should be given in the calculation and was selected as the input parameter (termed as the "imaginative contraction ratio"), though it would be determined by the size of the separation which in turn was a function of the pressure rise due to combustion. Figure 5 shows the mixture static temperature and pressure after the aerodynamic compression as functions of the imaginative contraction ratio in the M6S case. Ignition of the mixture within the engine requires a static temperature of about 1000 K. To achieve this temperature level, the imaginative contraction ratio should exceed 6, that is, the separation should occupy more than 5/6 of the flow pass, and the obtained static pressure was more than $4 \times q_{a1}$. This pressure level was not observed in the engine tests (see Fig. 3). Thus, aerodynamic compression through the precombustion shock system to attain shock-induced combustion was not realistic in the present conditions.

Next, a fraction of the mixture was assumed to burn within the separation region around the injector to simulate the ignition and flame-holding region within the real engine. A similar approach was used in [12] to attain ignition in one-dimensional scramjet combustor calculation at M8 flight conditions at a fixed fraction of 0.1. In the present study, the fraction of the initially reacted fuel flow rate to the total fuel flow rate was defined as initial combustion efficiency η_{ci}, the number being the subject for further discussion so that it was varied.

Figure 6 shows the relation between the initial combustion efficiency and the thrust increment for both the M6S and M6V cases. The consequent thrust reduction is also shown in the figure as a function of η_{ci}. No sizable pressure rise was attained within the diverging combustor in both cases at the value of η_{ci} less than 0.44. The thrust reduction rate was extremely large for η_{ci} between 0.44 and 0.48, because pressure rise due to combustion was attained within the diverging combustor in the M6S case but it was not in the M6V case. As pressure rise within the diverging combustor was also

Table 3 Calculated and measured thrust increments in both M6S and M6V cases

		Thrust with equilibrium calculation, $F/q_{a1}A_1$			Thrust with kinetic calculation, $F/q_{a1}A_1$			Experiment
Airflow condition	Equivalent ratio	Airflow	Combustion	$\Delta F/q_{a1}A_1$	Airflow	Combustion	$\Delta F/q_{a1}A_1$	$\Delta F/q_{a1}A_1$
M6S	0.33	0.066	0.258	0.192	0.066	0.250	0.184	0.179
M6V	0.33	0.070	0.243	0.173	0.070	0.226	0.156	0.150

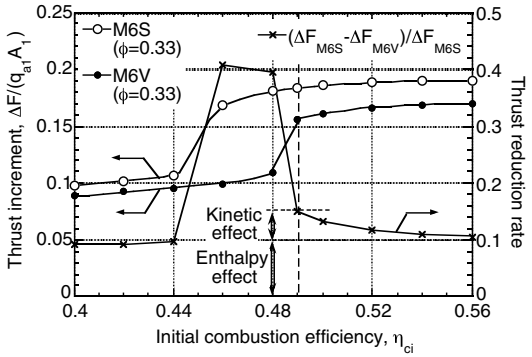

Fig. 6 Variations of thrust increment and thrust reduction with initial combustion efficiency.

attained in the M6V case in the experiment (Fig. 3), this regime was not our concern here. On the other hand, the thrust reduction rate was 0.10 at η_{ci} of 0.56. The thrust reduction was equal to the result by equilibrium calculation. Thus, in this regime, the reduction was caused by the difference in the flow condition, namely, the enthalpy.

The thrust reduction rate was 0.15 at η_{ci} of 0.49. Thus, the thrust reduction rate increased by another 0.05 above that due to the "enthalpy effect" (i.e., due to the difference in the flow condition). The cause of this additional decrease is clearly shown in Fig. 7, which shows static pressure distributions from the position of the injector. The peak pressure location in the M6V case shifted downstream by about 0.2 m due to a longer reaction time in comparison with the M6S case. This further downstream peak location resulted in a sizable decrease in the thrust increment in the M6V case, the reduction being denoted as the "kinetic effect" in Fig. 6. Again, the kinetic effect was mitigated with an increase in η_{ci} above 0.49, as the reaction time was shortened with further initial combustion and pressure rise due to heat release penetrating the constant area combustor in both cases.

The calculated thrust reduction rate of 15% at η_{ci} of 0.49 matched well with the experimental results shown in Table 3. In Fig. 7, the measured wall pressure distributions in both cases agreed with the calculated ones qualitatively, showing the delayed heat release and consequent delayed pressure rise in the M6V case. In a quantitative sense, there are discrepancies between the measured and calculated distributions, mainly due to 3-D effects such as rapid expansion at the onset of the nozzle, and occurrence of separation penetration into the constant area combustor in the M6S case. Despite these discrepancies, the thrust reduction was well represented with the one-dimensional analysis.

One interesting item is that $\eta_{ci} = 0.49$ matched with the predicted mixing efficiency at the exit of the constant area combustor through Eqs. (1) and (2). In a 3-D–CFD (computational fluid dynamics) study of the engine flowfield [17], the entire constant area combustor was covered by large separation regions and the majority of the heat release took place within the separation. Thus, it made sense to set the predicted mixing efficiency at the exit of the constant area combustor as the initial combustion efficiency, which denoted the flame-holding phenomena. In the case with a changed fuel flow rate in the following section, η_{ci} was given as the mixing efficiency at the exit of the constant area combustor through Eqs. (1) and (2) in accordance with the fuel flow rate. The overall mixing efficiency was also given through Eqs. (1) and (2).

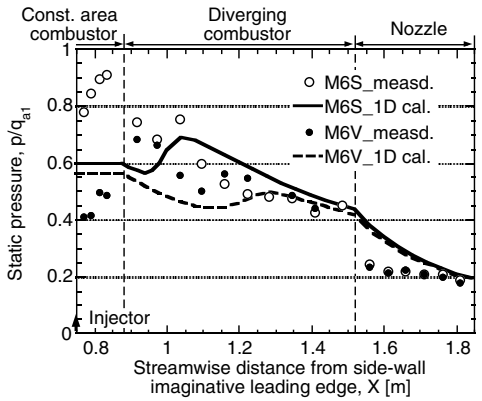

Fig. 7 Calculated static pressure distributions in the M6S and M6V cases with kinetic code.

V. Matching M6S and M6V Conditions

In this section, the engine test conditions were changed to eliminate the vitiation effects on engine performances by using the results of the one-dimensional analyses. This process will be useful for the interpretation of the engine test data with the vitiation to attain high enthalpy freestream in ground facilities.

A. Modifying the M6S Flow Condition (i.e., Flow Total Temperature)

In the above section, the difference in the flow states, namely, the flow enthalpy, was found to be responsible for the 2/3 of the thrust reduction. Thus, the flow condition was modified to attain matched flow conditions. The equivalence ratio was kept constant to be 0.33.

For simplicity of the calculation, the total temperature of the M6S flow was changed in the present study, while the mass flow rate was kept constant. Using the identical facility nozzle, this change in the total temperature would result in a change in the total pressure, and consequently, the static pressure of the supersonic freestream. In this study, the changes in the total temperature and the pressure were found to result in minor changes to the specific heat ratio and the boundary layer displacement thickness, so that the Mach number of the freestream should be almost identical regardless of the total temperature. Thus, the static pressure of the freestream p_{a1} at the target total temperature Tt_{a0} was calculated with the following simple equation based on mass flow conservation:

$$(p_{a1})/(p_{a1})_{\text{ref}} = [(Tt_{a0})/(Tt_{a0})_{\text{ref}}]^{1/2} \tag{3}$$

with the "reference" state being the actual test conditions shown in Table 1. The flow states were calculated then, with the flow rate, static pressure, and enthalpy as inputs.

Figure 8 shows the variation of the freestream total enthalpy, static temperature, and dynamic pressure with the total temperature of the M6S flow. The total enthalpy and static temperature in the M6V case were noted in the figure. As for the first step for trials, the total temperature of the M6S flow Tt_{a0S} was set to be 1530, 1590, or 1710 K, to attain the matched total temperature, the matched total enthalpy, or matched static temperature, respectively, to these M6V values. Additional Tt_{a0S} values were selected to enlarge the calculation domain.

For each Tt_{a0S} value, an equilibrium calculation was conducted to eliminate the enthalpy effect on the thrust reduction. Figure 9 shows the variation of the thrust increment against Tt_{a0S}. The thrust increment in the M6V case calculated with the equilibrium code is also shown as a reference. Though we expected the matched thrust performances at matched enthalpy conditions ($Tt_{a0S} = 1590$ K),

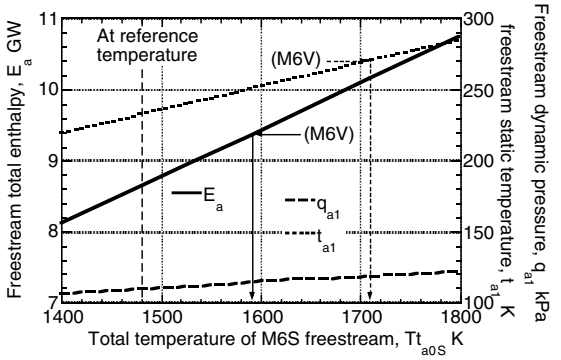

Fig. 8 Variations of flow enthalpy, static temperature, and dynamic pressure with M6S flow total temperature.

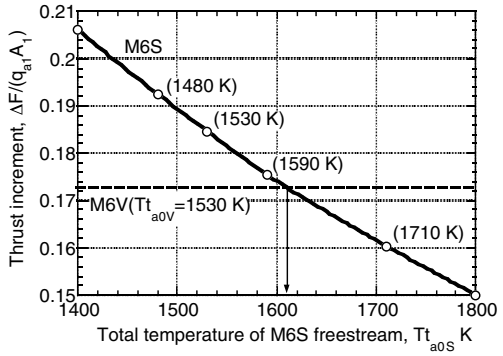

Fig. 9 Variations of thrust increment with M6S flow total temperature calculated with equilibrium code.

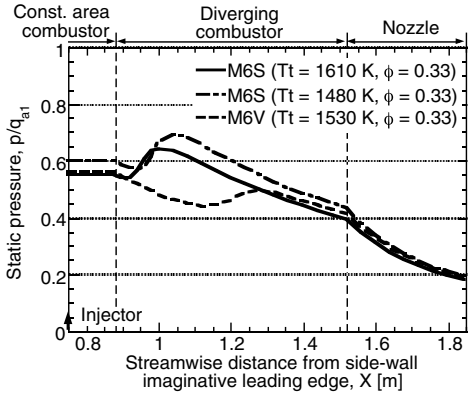

Fig. 10 Calculated static pressure distributions in the M6S and M6V cases with kinetic code at modified M6S total temperature.

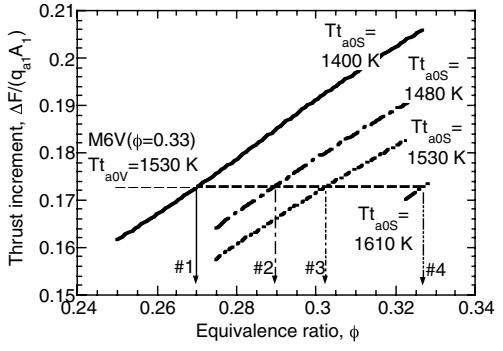

Fig. 11 Variations of thrust increment with equivalence ratio in the M6S case calculated with equilibrium code.

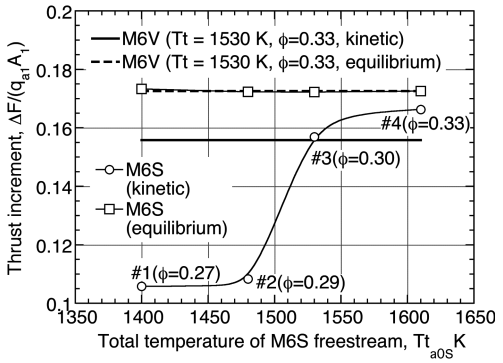

Fig. 12 Variations of thrust increment with M6S flow total temperature calculated with kinetic code.

there was a slight deviation, the difference in thermal properties and Mach number in both cases being the cause of the deviation. Consequently, the matched thrust increment to that in the M6V case was attained at Tt_{a0S} of 1610 K.

The rise in temperature level in the M6S case, however, should shorten the reaction time, which was expected to enhance the kinetic effect. Thus, kinetic calculations were conducted. Figure 10 shows the static pressure distribution for Tt_{a0S} of 1610 K. Those for the M6V case and original M6S case ($Tt_{a0S} = 1480$ K) are also shown in the figure. Because of the mitigation of the enthalpy effect, the pressure level in the modified M6S case ($Tt_{a0S} = 1610$ K) was reduced from that in the original M6S case ($Tt_{a0S} = 1480$ K), and was closer to that in the M6V case in the latter half of the diverging section. However, the peak pressure location shifted upstream as the reaction time was shortened, enlarging the kinetic effect. The resulting thrust reduction rate was 6%, a little bit larger than the kinetic effect in the original case.

B. Adjusting the M6S Test Conditions (i.e., Flow Total Temperature and Fuel Equivalence Ratio)

To mitigate both the enthalpy effect and the kinetic effect, we changed the fuel equivalence ratio as well as the M6S flow total temperature. As the enthalpy effect was more dominant, the equilibrium calculation was used to eliminate the enthalpy effects first. For a M6S flow total temperature, the fuel equivalence ratio was varied so that the resulting thrust increment would match with the equilibrium value in the M6V case. This calculation was repeated for several Tt_{a0S}. Figure 11 shows the calculation results, together with the equilibrium value in the M6V case. Note that the mixing efficiency was also varied in accordance with the equivalence ratio. As shown in Fig. 11, for example, the fuel equivalence ratio should be reduced from 0.33 to 0.29 in the case with Tt_{a0S} of 1480 K (original value) to attain a matched thrust increment to that in the M6V case.

As the next step, the kinetic calculation was carried out for several combinations of Tt_{a0S} and the equivalence ratio. The resulting thrust increments, shown in Fig. 12, were compared to the M6V value with the kinetic calculation. The results of the equilibrium calculations are also shown in the figure. For Tt_{a0S} below 1480 K, no effective heat release and consequent pressure rise were obtained within the diverging combustor or the nozzle. The thrust increment increased drastically with Tt_{a0S} at the regime of Tt_{a0S} greater than 1480 K. Because of the steeper expansion in the nozzle, the reaction zone found in the kinetic calculation could not be anchored within the nozzle, so that the rise in the increment from the bottom value meant that heat release and consequent pressure rise were attained within the diverging combustor. The increase in the increment with Tt_{a0S} meant that the reaction zone was advancing forward by shortening the reaction time. The obtained increment matched with the kinetic value in the M6V case at Tt_{a0S} of 1530 K. This Tt_{a0S} value was the same as the M6V value, however, we thought this was a mere coincidence. The increment kept on growing with Tt_{a0S} toward the equilibrium increment value of about 0.17 for the M6V case, with

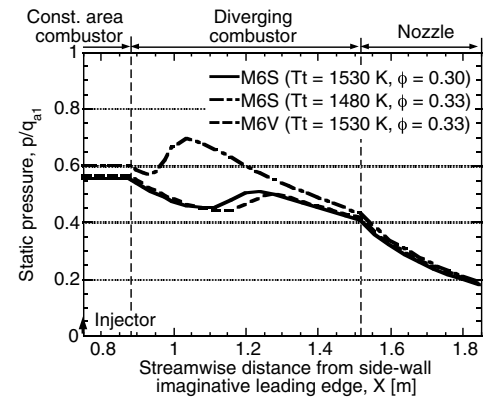

Fig. 13 Calculated static pressure distributions in the M6S and M6V cases with kinetic code at adjusted M6S test conditions.

Table 4 Summary of matched test conditions and predicted thrust production

						Flow states after init. reaction		Kinetic calc.
Airflow cond.	Total temp. Tt, K	Enthalpy E, GW	Equiv. ratio	Mixing eff.	Init. reaction eff.	p, kPa	t, K	Thrust increm., $\Delta F/q_{a1}A_1$
M6S	1530	9.0	0.30	0.88	0.50	61.6	1027	0.159
M6V	1530	9.4	0.33	0.87	0.49	61.3	1055	0.156

some saturating manner. The discrepancy was due to the incompleteness of the reaction.

Now, by adjusting the M6S test conditions (both freestream enthalpy and equivalence ratio), both the enthalpy effect and kinetic effect were eliminated. To confirm the equality of the combustion process within the engine in both cases, the static pressure distribution in the adjusted M6S case ($Tt_{a0S} = 1530$ K, $\phi = 0.30$) was compared to that in the M6V case in Fig. 13. The distribution in the original M6S case ($Tt_{a0S} = 1480$ K, $\phi = 0.33$) is also shown in the figure. Though there remained minor deviations, the distribution in the adjusted M6S case agreed well with that in the M6V case.

The adjusted M6S conditions as well as the M6V conditions were listed in Table 4 with the consequent engine performances. Also listed are the flow conditions after the initial combustion. Though the total temperatures matched with each other by coincidence, the static temperature of the mixture after the initial combustion should be higher for the M6V case to attain equivalent reaction time, because the higher concentration of water vapor tended to suppress the exothermic reaction in the M6V case. In the present case, the larger amount of the fuel equivalence ratio resulted in a larger amount of initial heat release to attain higher static temperature after initial combustion in the M6V case.

Through the adjustment procedure, the total temperature of the M6S flow was increased from the original value of 1480 K, while the decrease in the equivalence ratio resulted in the lower mixture temperature after the initial combustion and the consequent longer reaction time compared to those in the original conditions. The mixture temperature is also sensitive to the initial combustion efficiency so that a more detailed examination and modeling of the initial combustion (i.e., flame-holding phenomena) are necessary in future study.

In summary, we could establish a method to adjust the M6S test conditions, to duplicate the engine tests in the vitiated M6V conditions to those in the clean M6S conditions, with the rather simple one-dimensional analyses combining equilibrium and kinetic calculations. The exact matching should require real engine tests or 3-D CFD, but this analysis gave a good starting point for these more detailed and laborious analyses. Furthermore, an inverse procedure to the current analyses will give a way to convert the test data in the vitiated freestream conditions to those in the clean, flight conditions.

VI. Conclusions

Quasi-one-dimensional analyses were carried out to investigate the effects of vitiation on engine performance measured in the Mach 6 flight conditions obtained with two different heating methods, that is, with the storage heater (M6S case) or the vitiation heater (M6V case).

Effects of the airflow condition and reaction time on engine performance were examined and were modeled one dimensionally to show the following:

1) The difference in the freestream conditions, namely, the difference in the flow total enthalpy, was responsible for 2/3 of the reduction in the engine thrust production in the M6V case in comparison with the M6S case.

2) Shock-induced combustion due to aerodynamic compression through a precombustion shock system was not expected in the present M6 flight conditions.

3) About half of the fuel should be consumed in the flame-holding mechanism to attain effective heat release within the engine, the fraction being predictable with the simple empirical equation.

4) The longer reaction time in the M6V case was responsible for the remaining 1/3 of the reduction.

The M6S test conditions were adjusted to attain matched engine performance to that in the M6V case to show the following:

1) Matching the flow total enthalpy almost eliminated the effects of the differences in the flow conditions on the engine performance calculated with the equilibrium code, with a minor deviation left behind.

2) Besides the flow conditions, the fuel equivalence ratio should be adjusted to attain the matched engine performance calculated with the kinetic code.

Appendix: Validation of Simplification in Analyses

The present one-dimensional analyses were simplified to reduce the required calculation resources. The chief simplifications are 1) wall friction and heat transfer being neglected, and 2) constant mixing efficiency assumption throughout the combustor and nozzle sections. In this Appendix, these simplifications are validated in terms of the thrust reduction rate by using equilibrium calculations.

First, the impacts of the wall friction and heat transfer on the thrust reduction rate were examined. Skin friction and heat transfer were calculated for every step based on the one-dimensional mean flow states at the inlet of the control volume which was about 10 mm in length, with the van Driest method [18] and the Reynolds analogy. In the calculation, the mixing efficiency was set to be 0.87 throughout the combustor and nozzle sections. Table A1 shows the thrust increment for both M6S and M6V cases with or without wall friction/heat transfer, as well as the thrust reduction rate. The thrust increments were reduced by about 10% by taking both wall friction and heat transfer into account in the calculation. However, the estimated thrust reduction rate with the friction was almost identical to that without friction. Thus, neglecting wall friction and heat transfer had little effects on the M6S and M6V comparison in terms of the thrust reduction rate.

Next, the impacts of the nonuniformity in the streamwise mixing efficiency distribution were examined. The streamwise mixing efficiency shown by Eq. (1) was used for the equilibrium calculation, and obtained thrust increments as well as the thrust reduction rate were also summarized in Table A1. Though the nonuniformity in the streamwise mixing efficiency distribution had sizable effects on the

Table A1 Wall friction/heat transfer and η_m effects on thrust reduction

	τ_w & Q_w	η_m	$\Delta F_{\mathrm{M6S}}/q_{a1}A_1$	$\Delta F_{\mathrm{M6V}}/q_{a1}A_1$	$(\Delta F_{\mathrm{M6S}} - \Delta F_{\mathrm{M6V}})/\Delta F_{\mathrm{M6S}}$
Baseline case	w/o	Const.	0.192	0.172	10.4%
τ_w & Q_w effects	w/	Const.	0.174	0.154	11.5%
$\eta_m(x)$ effects	w/o	Equation (1)	0.173	0.156	9.8%

thrust increment, the resulting thrust reduction rate was almost insensitive to the mixing efficiency distributions.

Based on these validations, the wall friction and heat transfer terms were neglected, and a constant mixing efficiency with its value equal to that given at the engine exit through Eq. (1) was used in the one-dimensional calculation in the main text.

References

[1] Kanda, T., and Kudo, K., "Conceptual Study of a Combined-Cycle Engine for an Aerospace Plane," *Journal of Propulsion and Power*, Vol. 19, No. 5, 2003, pp. 859–867.

[2] Mitani, T., Tomioka, S., Kanda, T., Chinzei, N., and Kouchi, T., "Scramjet Performance Achieved in Engine Tests for M4 to M8 Flight Conditions," JAXA Research and Development Rept. JAXA-RR-03-020E, 2004; also available as AIAA Paper 2003-7009, Dec. 2003.

[3] Mitani, T., Hiraiwa, T., Sato, S., Tomioka, S., Kanda, T., and Tani, K., "Comparison of Scramjet Engine Performance in Mach 6 Vitiated and Storage-Heated Air," *Journal of Propulsion and Power*, Vol. 13, No. 5, 1997, pp. 635–642.

[4] Mitani, T., Chinzei, N., and Kanda, T., "Reaction and Mixing-Controlled Combustion in Scramjet Engines," *Journal of Propulsion and Power*, Vol. 17, No. 2, 2001, pp. 308–314.

[5] Pellett, G. L., Bruno, C., and Chinitz, W., "Review of Air Vitiation Effects on Scramjet Ignition and Flameholding Combustion Processes," AIAA Paper 2002-3880, 2002.

[6] Edelmann, R. B., and Spadaccini, L. J., "Theoretical Effects of Vitiated Air Contamination on Ground Testing of Hypersonic Airbreathing Engines," *Journal of Spacecraft and Rockets*, Vol. 6, No. 12, 1969, pp. 1442–1447.

[7] Srinivasan, S., and Erickson, W. D., "Interpretation of Vitiation Effects on Testing at Mach 7 Flight Conditions," AIAA Paper 95-2719, July 1995.

[8] Kishida, T., Tomioka, S., Hiraiwa, T., Kobayashi, K., and Yamasaki, H., "An Analytical Study of Scramjet Combustion at Mach 6 Flight Conditions," *AIP Conference Proceedings*, Vol. 832, May 2006, p. 461.

[9] Hiraiwa, T., Kobayashi, K., Tomioka, S., and Izumikawa, M., "Gas-Sampling Survey from Exhaust Flows in Scramjet Engines at Mach-6 Flight Condition," AIAA Paper 2004-3341, July 2004.

[10] Jachimowski, C. J., "An Analytical Study of the Hydrogen-Air Reaction Mechanism With Application to Scramjet Combustion," NASA Technical Paper 2791, 1988.

[11] Kanda, T., Hiraiwa, T., Mitani, T., Tomioka, S., and Chinzei, N., "Mach 6 Testing of a Scramjet Engine Model," *Journal of Propulsion and Power*, Vol. 13, No. 4, 1997, pp. 543–551.

[12] Diskin, G. S., and Northam, G. B., "Effect of Scale on Supersonic Combustor Performance," AIAA Paper 87-2164, 1987.

[13] Radhakrishnan, K., and Bittker, D. A., "LSENS, A General Chemical Kinetic and Sensitivity Analysis Code for Homogeneous Gas-Phase Reactions-II. Code Description and Usage," NASA RP-1329, Feb. 1994.

[14] Yatsunami, T., Mitani, T., Kobayashi, K., and Masuya, G., "Effects of Residual Radicals on Scramjet Engine Testing," *Journal of the Japan Society for Aeronautical and Space Sciences*, Vol. 48, No. 563, 2000, pp. 19–25 (in Japanese).

[15] Kanda, T., Watanabe, S., Hiraiwa, T., Izumikawa, M., and Mitani, T., "Measurement of Mass Capture Ratio of Scramjet Inlets," *Proceedings of the 42nd Conference on Aerospace Propulsion*, 2002, pp. 53–58 (in Japanese).

[16] Waltrup, P. J., and Billig, F. S., "Prediction of Precombustion Wall Pressure Distributions in Scramjet Engines," *Journal of Spacecraft and Rockets*, Vol. 10, No. 9, 1973, pp. 620–622.

[17] Kodera, M., Sunami, T., and Nakahashi, K., "Numerical Analysis of Combusting Flows in Scramjet," ISTS 2000-a-12, May 2000.

[18] van Driest, E. R., "Turbulent Boundary Layer in Compressible Fluids," *Journal of Aeronautical Sciences*, Vol. 18, No. 3, 1951, pp. 145–160.

R. Bowersox
Associate Editor